



Contents lists available at ScienceDirect

Remote Sensing of Environment

journal homepage: www.elsevier.com/locate/rse

Improving ground cover monitoring for wind erosion assessment using MODIS BRDF parameters

Adrian Chappell^{a,*}, Nicholas P. Webb^b, Juan Pablo Guerschman^{a,g}, Dean T. Thomas^c, Gonzalo Mata^c, Rebecca N. Handcock^{c,d}, John F. Leys^e, Harry J. Butler^f^a School of Earth and Ocean Science, Cardiff University, Cardiff CF10 3XQ, UK^b USDA-ARS Jornada Experimental Range, Las Cruces, NM, USA^c CSIRO Agriculture and Food, Private Bag 5, Wembley, WA 6913, Australia^d Murdoch University, 90 South St., 6150 Murdoch, WA, Australia^e Science Division, NSW Office of Environment & Heritage, PO Box 20, Gunnedah, NSW 2380, Australia^f School of Agricultural, Computational and Environmental Sciences, University of Southern Queensland, Toowoomba, Australia^g CSIRO Land and Water, GPO Box 1700, Acton ACT 2601, Australia

ARTICLE INFO

Keywords:

Ground cover

Lateral cover

Wind erosion

Albedo

MODIS

BRDF

Australia

USA

ABSTRACT

Measuring and monitoring controls on wind erosion can facilitate detection and prediction of soil degradation important for food security. Ground cover is widely recognised as an important factor for controlling soil erosion by wind and water. Consequently, maintaining ground cover (e.g., vegetation, crop canopy, crop residue) is a recommended management practice which is widely adopted by farmers and land owners. Wind erosion is a lateral or horizontal process and the amount of ground cover needed to maintain lateral cover ($L_c = nbh/S$ where n roughness elements occupy ground area S and have b and h mean breadth and height, respectively) is not well-established. Soil may be removed from beneath or between crop and natural vegetation canopies depending on the width, height and distribution of cover types relative to wind direction and strength. Monitoring by repeated measurement or estimation of ground cover provides information to develop an understanding of its spatial and temporal variation. Fractional cover (f_c) retrieved from optical satellite remote sensing (e.g., Moderate Resolution Imaging Spectroradiometer; MODIS) provides a consistent and repeatable measure of ground cover when viewed from above. Therefore, f_c provides an areal assessment of components of ground cover. Fractional cover is consequently not the most appropriate approximation of the protection of the soil from wind erosion. Extant wind erosion model parameterisations of L_c already benefit from the use of satellite-derived cover data (L_{fc}). However, the parameterisations are not well developed. Here, we address the need for a dynamic (multi-temporal), moderate resolution and global metric for wind erosion assessment and modelling. We demonstrate the benefits of using L_c within the context of monitoring ground cover for the assessment of wind erosion and review the basis for estimating ground cover using L_c . We describe a new method for an albedo-based approximation of aerodynamic sheltering (L_ω). We use ray-casting of rough surfaces from an existing wind tunnel study to establish a relation between measured L_c and directional hemispherical reflectance $\omega_{dir}(0^\circ, \lambda)$, the so-called ‘black-sky albedo’ and its inverse to estimate shadow. The relation is confirmed to be dependent on the solar zenith angle (θ) and spectral (λ) confounding factors (e.g., soil moisture, soil mineralogy). We reduced the λ dependency of $\omega_{dir}(0^\circ, \lambda)$ by normalising with the MODIS (MCD43A1) BRDF parameter f_{iso} to estimate albedo-based lateral cover (L_ω) globally over space (500 m pixels) and time (every 8 days). We compared L_ω with f_c and L_{fc} over time for selected locations in Australia and examined L_ω across Australia and the USA using national biogeographic regions. Consistent with current approaches to estimating L_c , our results were not field validated due to the dearth of ground-based measurements. However, our results demonstrate that L_ω will improve wind erosion models particularly over large areas and L_ω is likely to be a valuable source of decision-support information to guide policy makers and land managers on where, when and how to reduce wind erosion.

* Corresponding author.

E-mail address: chappella2@cardiff.ac.uk (A. Chappell).<http://dx.doi.org/10.1016/j.rse.2017.09.026>

Received 20 September 2016; Received in revised form 11 September 2017; Accepted 20 September 2017

0034-4257/ Crown Copyright © 2017 Published by Elsevier Inc. All rights reserved.

1. Introduction

Wind erosion is a major driver of soil degradation particularly in the world's drylands (Lal, 2001; Ravi et al., 2010). Wind erosion and dust emission promote the loss of soil organic carbon and soil nutrient decline (e.g., Li et al., 2008; Chappell et al., 2013; Webb et al., 2012), impact land productivity (Lal, 1998; den Biggelaar et al., 2003a, 2003b; Sterk et al., 1996) and influence global terrestrial and marine biogeochemical cycles and climate (Calvo et al., 2004; Jickells et al., 2005; Shao et al., 2011). By the end of this century, drylands are expected to increase to cover half of the Earth's land surface (Huang et al., 2016). Increased aridity enhanced by warming and a rapidly growing human population are expected to increase land degradation and decrease food security particularly in the drylands of developing countries (Huang et al., 2016). Measuring and monitoring controls on wind erosion can facilitate detection and prediction of soil degradation, providing a basis for improved land management and understanding dust impacts downwind (McTainsh et al., 1990; Koch et al., 2015). Detection and prediction remain challenging prospects for broad scale (regional to national) monitoring and assessment (McTainsh et al., 1990; Webb et al., 2009). Remote sensing has been key to improving wind erosion and dust emission model capabilities for some time (Shao et al., 1996), and have been used to inform management and policy (State of the Environment 2011 Committee, 2011; US Department of Agriculture, 2015). These models require information on structural characteristics of soil and vegetation that attenuate the aerodynamics of the land surface and the soil susceptibility to erosion (Chappell et al., 2006, 2007). The most successful models have exploited multi-temporal remote sensing data to represent dynamic land surface conditions that control the location and timing of wind erosion and dust emission (Shao, 2000; Marticorena and Bergametti, 1995). Further integrating remote sensing products into wind erosion models is expected to improve model fidelity and substantially reduce the uncertainty in predictions (Chappell et al., 2010).

Wind erosion and dust emission occur when there is a coincidence of sufficiently strong winds (wind erosivity) and a soil surface which may be eroded (soil erodibility). Soil erodibility is controlled by soil grain size and cohesion, which vary considerably in space and time in response to soil moisture, physical and biological crusting and disturbance (Webb and Strong, 2011). Wind erosivity is moderated by roughness features that control the land surface aerodynamics (Raupach et al., 1993). In agricultural regions, roughness is dominated by crops, pastures and oriented soil ridges with various heights, widths and spacing. In rangelands, roughness is characterised by the heterogeneous and anisotropic (i.e., clumped) distribution of vegetation with different growth forms and the varied phenology of vegetation growth and responses to management (Gillette et al., 2006). Perhaps the greatest challenge for wind erosion monitoring and prediction is to characterise and represent these land surface controls on the erosion process across the continuum of land surface roughness from homogeneous to heterogeneous and from static to dynamically changing. While advances have been made in capturing surface roughness effects on wind erosion through remote sensing, substantial limitations remain with the approach and the parameterisation.

Ground cover is a proxy for roughness in wind erosion models (Shao, 2000) and is used to monitor the susceptibility of the land surface to wind erosion. Ground cover is defined here as vegetation (living and dead), biological crusts and stone that is in contact with the soil surface (Muir et al., 2011; Herrick et al., 2017). Maintaining ground cover to protect soil from erosion is a recommended management practice which has been adopted by farmers and land users (Leys, 1991; Li et al., 2007). Felton et al. (1987) suggest that prevention of wind erosion requires 70% ground cover of cereal residue fixed to the soil. The maintenance of adequate ground cover of at least 50% on average across a field is recommended to protect soil against wind erosion (Leys et al., 2009). However, this threshold is a general rule used for

agricultural extension purposes. It does not account for different wind speeds, roughness configurations and structures, or for different wind directions and seasons.

Considerable effort has recently been devoted to deriving products representing the fractional ground cover (f_c) of photosynthetic vegetation (PV), non-photosynthetic vegetation (NPV) and bare soil (BS, including stones and rock) using hyperspectral and multispectral sensors (e.g., Guerschman et al., 2015 their Table 1). The availability of fractional cover products in Australia at moderate spatial (e.g., 500 m) and temporal (8–16 day) resolutions, provide the means of accounting for horizontal (planform) cover, thus enabling ground cover monitoring and the effects of climate variability and land management on wind erosion to be assessed (Stewart et al., 2011). However, soil erosion is a primarily lateral process and wind erosion in particular may occur beneath tall vegetation and crop canopies and between some types of ground cover (Bergametti and Gillette, 2010). Fractional cover f_c does not capture the effects of cover (roughness) structures projected into the airstream, or its interactive effects due to its 3-dimensional spatial distribution. These factors substantially affect land surface aerodynamics and rates of wind erosion. For example, the 'green' (PV) f_c has been used with vegetation height classifications to approximate the frontal area of vegetation as input to drag partition schemes that represent the aerodynamic effect of vegetation on wind momentum (Shao et al., 1996). We contend that, because of the reliance on f_c , current approximations of land surface aerodynamics generate large uncertainties in wind erosion assessments. New metrics that account for the vertical structure and distribution of surface roughness are urgently needed to improve the accuracy of wind erosion monitoring and prediction (Webb et al., 2014).

This paper addresses the need for a dynamic (multi-temporal), moderate resolution (500 m) and broad-scale (national) metric for representing the aerodynamic roughness of the land surface for wind erosion monitoring and models. The aim of the research is to develop estimates of lateral cover (L_c), a horizontal projection of the lateral density of roughness across the land surface, using the Moderate Resolution Imaging Spectroradiometer (MODIS). We begin by defining L_c and its use in existing wind erosion models. We establish an empirical relation between L_c and the albedo of rough surfaces, normalised to remove spectral influences, and demonstrate how the relation is general and universal for surfaces comprised of mixed spectral signatures from plants and soil. We then show how MODIS data can be used to estimate lateral cover and thereby satisfy the requirement for large area assessment of vertically- and horizontally-projected land surface aerodynamic roughness. We apply the new approach to a MODIS time series for selected land cover types in Australia, then map MODIS global L_c and explore how the new data can be used to improve ground cover monitoring and modelling of wind erosion.

2. Background to methodology

2.1. Aerodynamic roughness and lateral cover

Surface roughness includes erodible and non-erodible features of the land surface, such as living or dead vegetation and rocks. It also includes erodible features such as soil aggregates and ridges that change in size, shape and distribution in response to weather and land management. Surface roughness influences wind erosion by: (a) directly sheltering the soil surface from erosive winds; and (b) absorbing a portion of the wind momentum flux, thus reducing the wind erosivity (shear stress) at the soil surface (Marshall, 1971; Raupach et al., 1993). The direct sheltering effect of vegetation is captured in part by the area of ground covered by vegetation, but this measure does not account for the additional sheltering that occurs in the lee of standing roughness or the absorption of wind momentum. This sheltering constitutes areas of flow separation downwind of roughness elements (Arya, 1975) and may incorporate other roughness elements depending on the wind direction

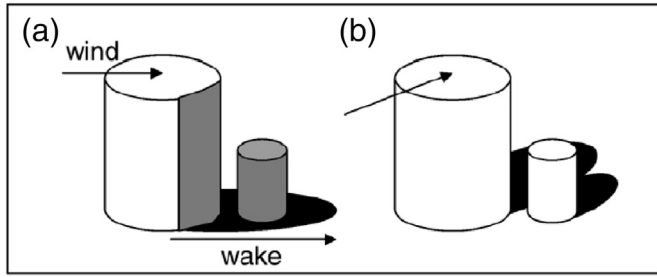


Fig. 1. Cylinders used to represent non-erodible roughness elements, protect a portion of the substrate surface that may include all or part of other roughness elements in a heterogeneous surface (a). A change in wind direction redefines the protected substrate and may expose previously protected roughness elements (b; reproduced from Chappell et al., 2010). The fractional cover of the roughness elements is the same in both cases, while their aerodynamic effect would be significantly different.

(Fig. 1). Therefore, momentum absorption is a function of the drag created by surface roughness and so varies with roughness element size, morphology, porosity, density and distribution (Brown et al., 2008). These factors controlling wind erosion processes are typically parameterised with lateral cover (defined next) in wind erosion models using vegetation indices. The lateral cover parameter is omitted or excluded from wind erosion assessment and monitoring because of the reliance on fractional ground cover.

Lateral cover (L_c , dimensionless; also known as roughness density or the frontal area index), is defined as:

$$L_c = \frac{nbh}{S}, \quad (1)$$

where n roughness elements occupy ground area S and b and h are their mean breadth and height, respectively. The measure is insensitive to roughness configuration, and therefore omits the effect of configuration on wake interactions in the lee of roughness elements and the spatial distribution of drag on the land surface (Webb et al., 2014). Lateral cover is labour-intensive to measure *in situ*, is difficult to measure in a rapid and repeatable way, and is therefore typically excluded from routine ground-based monitoring and validation studies. While the height and canopy gap-size distribution of vegetation can be measured in the field, and are used routinely for monitoring (e.g. Toevs et al., 2011; Herrick et al., 2017), methods are yet to be established for obtaining these data from remote sensing at broad (i.e., regional and national) spatial scales. Estimates of lateral cover retrieved from satellite data remains a practical solution for representing the effects of surface roughness on wind erosion.

For wind erosion models, L_c has previously been estimated (henceforth traditional approach) using a relation with vegetation cover (L_{fc}). For example, Shao et al. (1996, 2007) estimates it as:

$$L_{fc} = -c \ln(1 - a_c) \quad (2)$$

where c is an empirical coefficient which represents the shape of the vegetation type and a_c is the cover fraction (without distinction between fractional components of PV and NPV). The parameter $c = 0.35$ was determined empirically from a field in Australia with a wheat stubble (Shao et al., 1996). In practice, this parameter value is held constant in the absence of any other information about vegetation type (Darmenova et al., 2010). Alternatively, L_c may be estimated from the leaf area index (LAI)

$$L_{LAI} = \gamma_a LAI \quad (3)$$

where γ_a is a coefficient which represents the drag of differently shaped roughness elements i.e., ball-shaped plants have $\gamma_a = 1$, while tall plants $\gamma_a > 1$ and flat plants $\gamma_a < 1$. It remains challenging to classify large areas of vegetation according to their structure. However, there are

similarities between these metrics (Eq. (1)–(3)) and the Bi-directional reflectance distribution function (BRDF) shape parameters from different types of roughness elements used as shadow casters in albedo modelling (e.g., Wanner et al., 1995).

2.2. The relation between aerodynamic sheltering and albedo

Chappell and Heritage (2007) introduced the notion of using shadow to approximate sheltered areas and aerodynamic turbulence primarily because of the need to make estimates of sediment transport by wind for heterogeneous roughness across spatial scales. They suggested, following Arya (1975) and Raupach (1992), that the length of a sheltered area behind an isolated obstacle was a function of both wind velocity (at a reference height) and roughness element height. Chappell and Heritage (2007) calculated the sheltered area as shadow by invoking relative roughness to approximate the illumination angle. They showed a strong relation ($R^2 = 0.91$) between shadow and wind tunnel estimates of aerodynamic roughness length (z_0) obtained by Dong et al. (2002).

Monteith and Unsworth (2008) described a general increase in z_0 in the presence of vegetation and a decrease in albedo. Chappell et al. (2010) reconstructed the configurations of hemispheroids used to represent surface roughness in the wind tunnel study of Dong et al. (2002) and illuminated the surfaces for a range of zenith angles (for a given azimuth angle). The integration of all illumination angles approximated the single scattering albedo, and was strongly ($RMSE = 0.0026$) related to z_0/h . Using the same approach with a digital elevation model of a natural surface, the shadow was shown to be a function of both zenith and azimuth angles. This illustrated the anisotropic nature of z_0 and the predictive power of the shadow. Cho et al. (2012) suggested that z_0 and albedo are related by the structure of the vegetation which changes radiation penetration and influences wind drag. They demonstrated a strong relation between z_0 and albedo ($R^2 = 0.76$; $p < 0.0001$). However, when z_0 was scaled by object height (z_0/h) as is done traditionally, the relation with albedo was poor showing that h is a considerable source of uncertainty.

Marshall (1971) demonstrated how drag is partitioned over surfaces with a range of L_c and roughness configurations. That experiment is regarded as seminal in the wind erosion community and has been used to develop and evaluate drag partition models (Raupach et al., 1993; Walter et al., 2012). Marshall's (1971) study used mainly cylinders but some hemispheres, all of height $h = 2.54$ mm with several diameters (b) and modified the edge-edge spacing (B) to produce isotropic surfaces with a range of configurations (b/h and B/h) and lateral cover. Marshall (1971) used B/h ratios of the roughness arrays from 1 to 59 and suggested that b/h ratios between 1 and 3 are common to many woody perennial plants while cylindrical and hemispherical morphologies occur frequently. Walter et al. (2012) suggested that semi-arid, shrub-dominated communities, common in wind-eroding drylands, are rarely more closely spaced than an average B/h of 2. They demonstrated using a wind tunnel study of live plants that cylinders were an adequate approximation of the aerodynamic behaviour of the plants. However, cylinders produce an artefact when illuminated because of their bluff wall and horizontal top and are not representative of the structures, particularly in soil, found in the field. Wanner et al. (1995) and Cierniewski (1987) used hemispheres and hemispheroids to represent surface light scatterers.

3. Methods

3.1. Ray-tracing to estimate shadow

Consistent with this last approach we replaced the cylinders of Marshall's (1971) study with hemispheroids of the same dimensions.

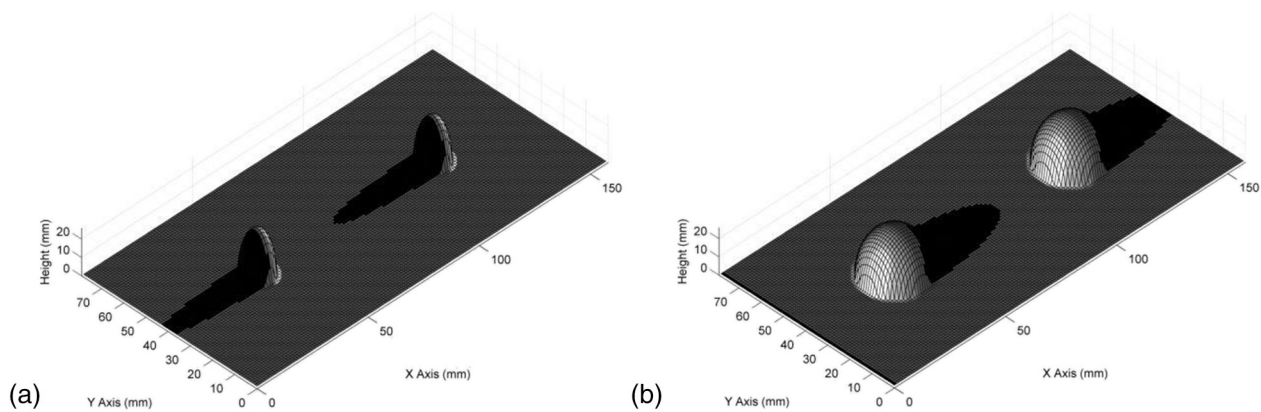


Fig. 2. Digital elevation models representing Marshall's (1971) surfaces (a) $b/h = 0.5$; $B/h = 2.5$; (b) $b/h = 1$; $B/h = 2$ illuminated at $\theta = +60^\circ$ and $\theta = -60^\circ$, respectively.

Notably, this replacement makes no difference to the calculation of lateral cover since the maximal dimensions of a cylinder and a hemispheroid are identical. We calculated L_c using Eq. (1) from the geometry of surfaces of objects created in Marshall's (1971) wind tunnel study.

Using a digital elevation model, we reconstructed the roughness of each surface of objects used in Marshall's (1971) wind tunnel study. The shadow and brightness of the surface was estimated following the ray-casting approach (at-nadir view) of Chappell et al. (2010). A light ray was cast separately from many illumination angles (θ) and where these rays were intercepted on either the roughness elements or the background plane they were designated as lit. Shadows were identified along a ray path 'downstream' of its interception by a roughness element. When viewed at nadir, the number of pixels that were lit or in shadow were summed separately and divided by the total number of pixels to produce the ratio $\rho(\theta)$. We integrated ρ over all θ ($0-90^\circ$), assumed an isotropic response and approximated the direct beam (*dir*) directional (at-nadir view) hemispherical albedo $\omega_{dir}(0^\circ, \lambda)$ for a given waveband, λ . Fig. 2 provides two examples of digital elevation models of Marshall's surfaces which were illuminated using this ray-casting approach.

In addition to the surface roughness or structural influences on albedo there are many other surface characteristics that may influence the albedo including soil moisture content, organic matter content, and iron-oxides. Many of these factors are confounding as illustrated by the study of Coulson and Reynolds (1971). They showed that the albedo of a dry 'disked' soil surface was as small as that of a wet flat surface, but a dry puddled surface had nearly double the albedo. To remove the spectral signal we calculated the shadow as the inverse of albedo $1 - \omega_{dir}(0^\circ, \lambda)$ and then normalised that by the directional reflectance viewed and illuminated at nadir $\rho(0^\circ, \lambda)$:

$$\omega_n = \frac{1 - \omega_{dir}(0^\circ, \lambda)}{\rho(0^\circ, \lambda)} = \frac{1 - \omega_{dir}(0^\circ)}{\rho(0^\circ)}. \quad (4)$$

To simulate the spectral influences in the ray-casting, we chose values for the reflectance of the pixel components which were broadly consistent with the descriptions in Dickinson (1983); Fig. 3 of albedo for wet and dry soil and vegetation. Consequently, the plane background (A_g) was allowed to vary between e.g., a wet, dark soil ($\rho = 0.1$) and a dry, bright sand ($\rho = 0.6$). Similarly, the roughness elements (A_c) were varied between $\rho = 0.6-0.1$ to represent bright to dark vegetation. These experiments were therefore designed to show how the relation between ω and L_c was influenced by other spectra-dependent factors such as soil moisture, mineralogy and vegetation type.

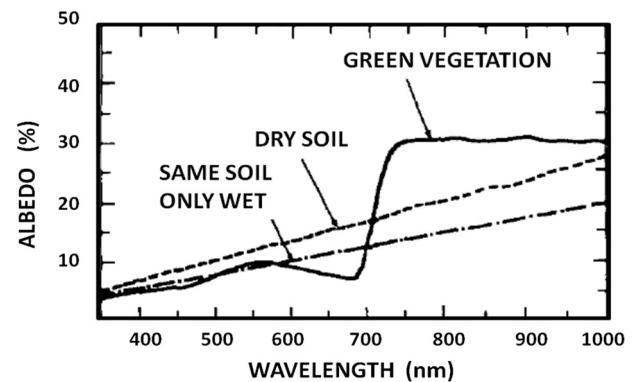


Fig. 3. Spectra-dependent albedo for some pertinent land surface characteristics (reproduced from Dickinson, 1983 their Fig. 1).

3.2. Estimating aerodynamic sheltering from MODIS direct beam (L_ω)

Accurate detection and quantification of change at the Earth's surface over time and space requires removal of the confounding effects of geometric distortion, radiometric variability, angular illumination and observation geometry and cloud, shadow and water contamination from imagery (Scarath et al., 2010). Surface structure influences the bi-directional reflectance for example by shadow-casting, mutual view shadowing and the effects of the spatial distribution of vegetation elements. Surface optical characteristics also effect the bidirectional reflectance distribution function (BRDF) of the surface, for example via vegetation-soil contrasts and the optical attributes of canopy elements (Lucht et al., 2000). Surface roughness (from vegetation, soil etc.) has long been recognised to be of significance for the scattering of reflected light and in creating shadows which considerably reduce reflectance (cf. Hapke, 1993; Tsvetsinskaya et al., 2002). Bi-directional soil reflectance models can be used to characterise the structure (roughness) and composition of bare soils (Cierniewski, 1987; Pinty et al., 1989; Jacquemoud et al., 1992; Chappell et al., 2006, 2007).

As a consequence, the spatial and temporal distribution of these land surface properties, as seen in the observed BRDF and albedo, represent a variety of natural and human influences in the land surface e.g., agricultural practices such as harvesting, vegetation phenology, vegetation cover changes (Lucht et al., 2000). The operational MODIS BRDF/albedo algorithm makes use of a kernel-driven linear BRDF model, which relies on the weighted sum of an isotropic parameter (f_{iso})

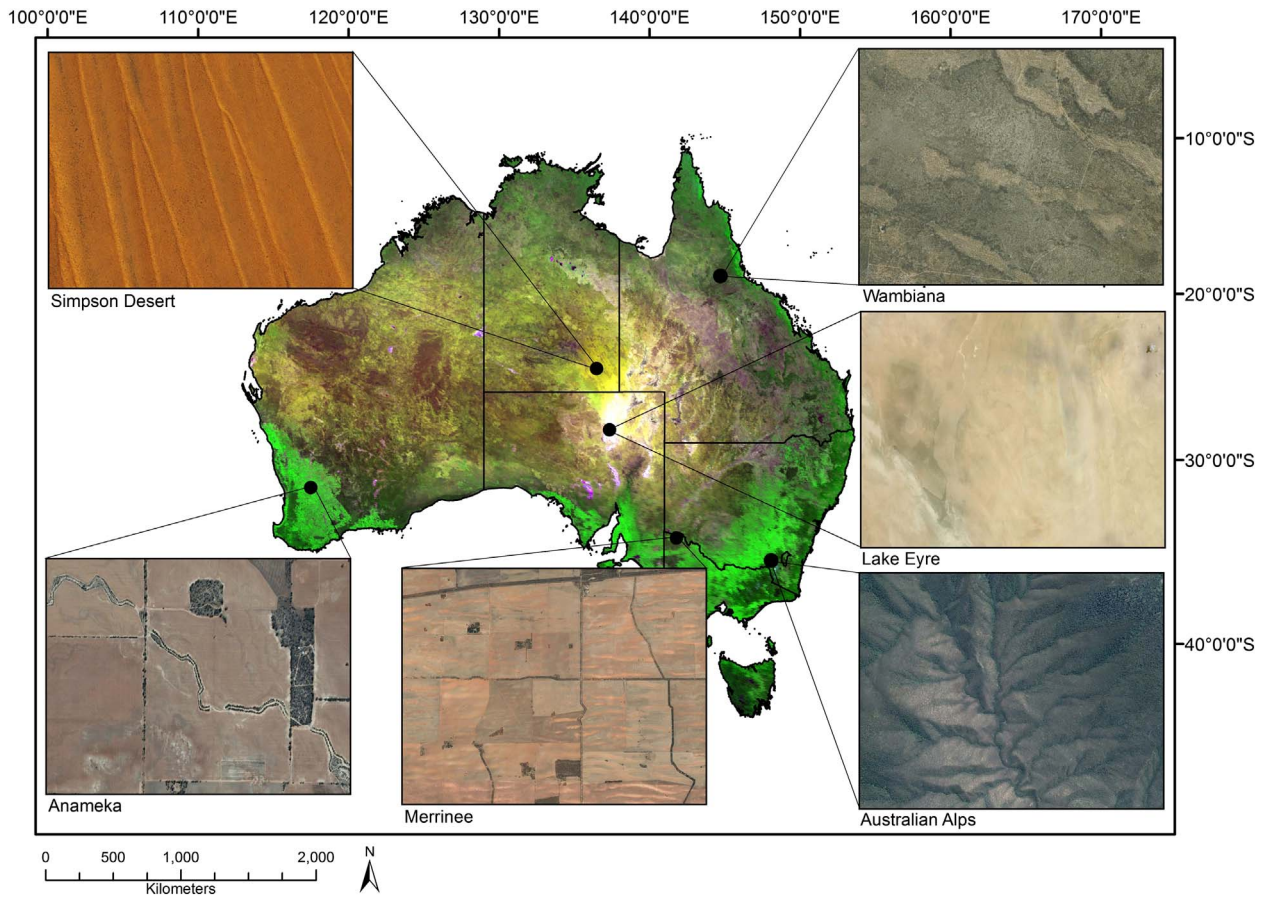


Fig. 4. Location of selected pixels (500 m) across Australia where the time series of agro-ecological regions are summarised on average monthly and yearly for the duration of the archive from 2000.

and two functions (or kernels) with parameters (f_{vol} and f_{geo}) of viewing and illumination geometry (Roujean et al., 1992). The parameter f_{iso} represents the spectral contribution, while f_{vol} is the volumetric scattering (e.g., by leaves and grass) and f_{geo} represents the scattering due to objects like shrubs, bushes and trees. The kernel weights that best fit the majority situation are selected (Lucht et al., 2000; Schaaf et al., 2002) and used to produce the at-nadir BRDF-adjusted reflectance (NBAR) product (MCD43A4). Once an appropriate BRDF model has been retrieved, integration over all view angles results in a directional-hemispherical ‘black-sky’ albedo called the direct beam (dir). It is a spectral-dependent (λ) direct beam albedo $\omega_{dir}(\theta, \lambda)$ and a function of solar zenith angle θ in the absence of a diffuse component.

The MODIS albedo product (MCD43A) provides 500 m data available every 8 days with 16 days of acquisition from the year 2000. The product provides ‘black-sky’ and ‘white-sky’ albedo for wavebands (λ) 1–7 (1: 620–670 nm; 2: 841–876 nm; 3: 459–479 nm; 4: 545–565 nm; 5: 1230–1250 nm; 6: 1628–1652 nm; 7: 2105–2155 nm) and three broad bands (VIS 0.3–0.7 μ m, NIR 0.7–5.0 μ m, and Shortwave 0.3–5.0 μ m) in a Level 3 gridded dataset with a Sinusoidal projection. We extracted from the MODIS archive for Australia the MODIS BRDF parameters and ‘black-sky’ albedo at-nadir (local solar noon) illumination angle, and the integration of view angle information. We assumed that the MODIS $\omega_{dir}(0^\circ, \lambda)$ was reciprocal to our ray-casting model which used at-nadir view angle and integrates illumination

angle.

To make use of the MODIS black sky albedo and estimate lateral cover, we need to remove the influences of the spectrally-dependent factors. For a given scene, soil moisture or soil composition may vary across space and therefore explain some of the variation in albedo which we intend to attribute to roughness. Similarly, over time a pixel may show changing albedo due to changing roughness but which will be confounded by changing albedo due to e.g., soil moisture. We normalised the shadow $1 - \omega_{dir}(0^\circ, \lambda)$ by dividing it by the MODIS isotropic parameter f_{iso} to remove the spectral influences. This was suggested by Crystal Schaaf and colleagues from the MODIS team because that parameter was designed to contain information on spectral composition as distinct from structural information.

$$\omega_n = \frac{1 - \omega_{dir}(\theta, \lambda)}{f_{iso}(\lambda)} = \frac{1 - \omega_{dir}(\theta)}{f_{iso}} \quad (5)$$

We also normalised $1 - \omega_{dir}(0^\circ, \lambda)$ by NBAR for a given λ to investigate the difference with the previous approach:

$$\omega_n = \frac{1 - \omega_{dir}(0^\circ, \lambda)}{NBAR(\lambda)} = \frac{1 - \omega_{dir}(0^\circ)}{NBAR} \quad (6)$$

To predict lateral cover L_c we needed to make the MODIS-based ω_n consistent with the calibration relations established from the ray-

Table 1
Characteristics of pixels used to describe the temporal dynamics of typical agro-ecological regions across Australia.

Location, state	Land cover/land use	Characteristics
Wambiana (long-term grazing trial), North Queensland	Tropical savanna/cattle grazing	The Wambiana grazing trial started in 1997 to test and develop sustainable and profitable strategies to manage for rainfall variability in extensive grazing lands and over-grazing and soil erosion.
Simpson Dunes, Queensland	Old, low-angle dune system with minimal vegetation cover/cattle grazing	Large area of dry, red sandy plain and dunes in Northern Territory, South Australia and Queensland in central Australia.
Lake Eyre, South Australia	Typically, dry lake bed with little vegetation cover/desert ecosystem	Periodically inundated salt pan. During dry periods can be a major dust source.
Australian Alps, New South Wales	<i>Eucalyptus</i> spp. forest often with closed canopy/reserve	The highest mountain range in Australia located in southeastern Australia, and it straddles eastern Victoria, southeastern New South Wales, and the Australian Capital Territory.
Merrine, Mallee, Victoria	Agricultural region typically combining wheat cultivation and sheep grazing.	First cleared after World War II and produced considerable wind erosion; soil conservation has been slowly adopted and wind erosion and dust emission remains a substantial land management issue.
Anameka, Western Australia	Agricultural region typically combining wheat cultivation and sheep grazing	Another wind erosion hotspot due to sandy soils and land management issues.

casting and Marshall's (1971) wind tunnel. We therefore translated and scaled the data (ω_{ns}) from the MODIS range (ω_{nmin} , ω_{nmax}) to that of the calibration data ($a = 0$ to $b = 1$) using the following equation:

$$\omega_{ns} = \frac{(a - b)(\omega_n(\lambda) - \omega_n(\lambda)_{max})}{(\omega_n(\lambda)_{min} - \omega_n(\lambda)_{max})} + b. \quad (7)$$

We processed the current MODIS (MCD43A1) archive for Australia to estimate $\omega_{ns}(f_{iso}, \lambda)$ using Eqs. (5)–(7). We then used the calibration (between measured L_c (Marshall, 1971) and the ω_n from ray-casting) to predict lateral cover from MODIS albedo (L_ω). We expected a priori that the most suitable approach to estimating L_c would be that which did not vary with waveband and which matched approximately the patterns evident from estimates of fractional cover. Consequently, we investigated these assumptions using three different λ (1: 620–670 nm; 3: 459–479 nm and 7: 2105–2155 nm) and available fractional cover data for Australia (Guerschman et al., 2009).

3.3. Evaluation of albedo-derived aerodynamic sheltering (L_ω)

There is no comprehensive dataset to evaluate the retrieval of L_ω from MODIS data. This is because L_c is not routinely measured on the ground. Intensive ground measurements in Australia (e.g., the Statewide Landcover and Trees Study; SLATS; ABARES, 2012) used to validate fractional cover data do not include measurements that are sufficient to calculate L_c . This is partly because of the lack of awareness of the need for these L_c data for erosion assessment, and also partly because the measurements for L_c are labour-intensive and therefore expensive to acquire. Where L_c has been measured (outside Australia), they were obtained for only a few, small areas (< 500 m pixel) (e.g., Marticorena et al., 2006; Pierre et al., 2014). These measurements would not provide a reliable information source for comparison at the scale of our MODIS-derived L_c , and offer less of a range in L_c values than the wind tunnel surfaces we used. Consequently, we propose to evaluate our estimates of L_ω by comparison with fractional cover (f_c) and

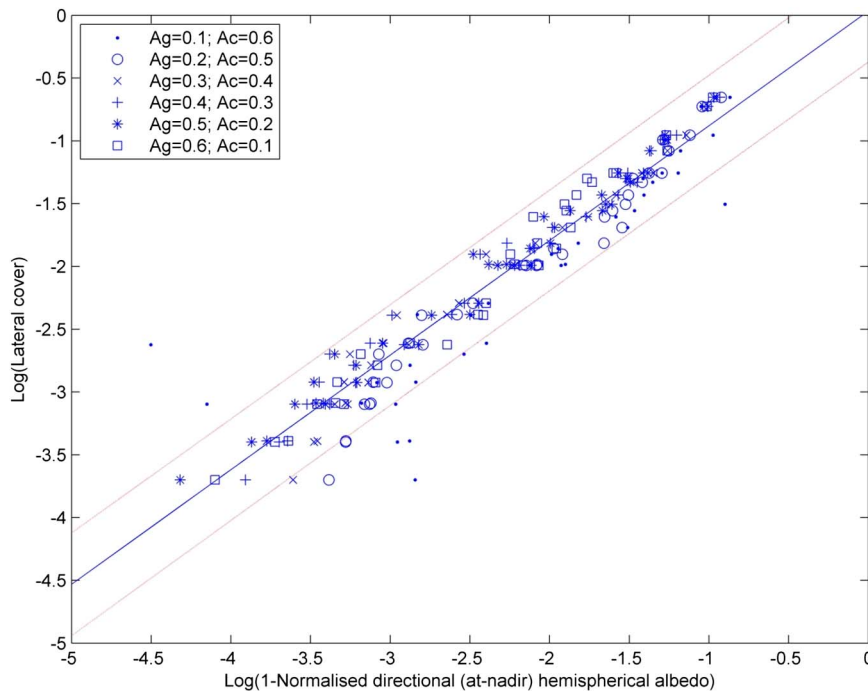


Fig. 5. Relation between lateral cover and the ratio of the directional (view at nadir) hemispherical shadow and the normalised directional hemispherical albedo for a range of reflectance of the plane background (A_g) and the roughness element (A_c) surfaces of cylinders and hemispheres used in the wind tunnel study of Marshall (1971). The reflectance of shadow was assumed to be 0.01 following photometric modelling (Hapke, 1993). The fitted function passes through the results and the 95% confidence intervals are also shown.

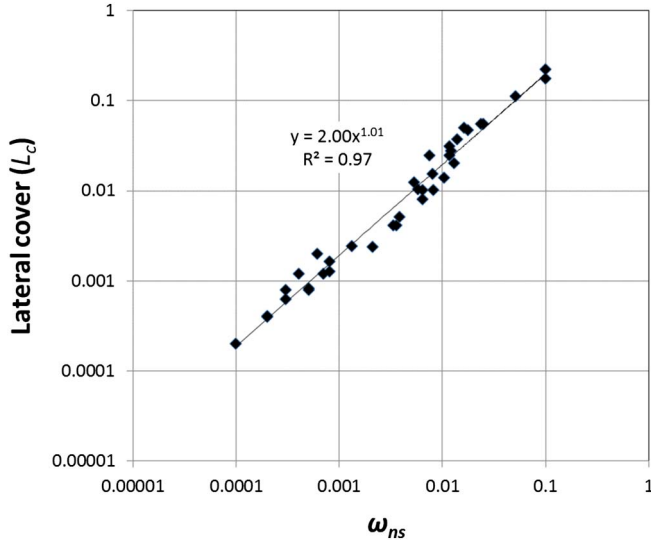


Fig. 6. Relation between normalised and rescaled albedo (ω_{ns}) and measurements of lateral cover (L_c) from Marshall's (1971) surface roughness. A simple power model is fitted using linear least squares regression.

L_{fc} .

MODIS-derived f_c data for Australia are routinely processed following the approach of Guerschman et al. (2009) and made publicly available (<http://www.auscover.org.au>). From this archive, we extracted maps of the fractional cover of photosynthetic (PV), non-photosynthetic (NPV) and bare soil (BS), to calculate L_{fc} (using Eq. (2)) and to describe for Australia their spatial variation for selected points in time. We also chose six locations (pixels) around Australia to represent characteristic land surface types (vegetation communities and soils; Fig. 4; Table 1). For each pixel, we retrieved an 8-day time series (ca 25,000 days) of each property (f_c , L_{fc} and L_ω) and summarised those data using averages over months and years for the entire length of time series (2000–2015). This provided a description of the temporal dynamics of the properties with respect to known seasonal vegetation responses at each location.

We predicted L_ω globally and evaluated its spatial patterns in the

context of global MODIS land cover classes (MCD12Q1; Friedl et al., 2010). We then examined the spatial patterns of L_ω at the national scale for Australia using the Interim Biogeographic Regionalisation for Australia (IBRA; Department of the Environment and Energy, 2016) and for the United States of America (USA) using the Major Land Resource Area (MLRA; USDA NRCS, 2006) classification systems which are commonly applied to structure national rangeland and cropland monitoring and management programs.

4. Results

4.1. Modelling aerodynamic sheltering (L_ω)

Fig. 5 shows the relation between measured lateral cover and normalised at-nadir hemispherical albedo ω_n . The relation appears robust to simulated differences in reflectance. Small L_c (sparse objects) have small ω_n and as L_c increases (objects are more closely spaced) ω_n increases. These results suggest that the normalisation removed the spectral dependence. We confirmed this by creating a plane background of the spectral characteristics of a soil using the main MODIS wavebands (Red = 0.25, NIR = 0.33, SWIR_{1.6} = 0.38 and SWIR_{2.2} = 0.10) and gave the roughness elements the spectral characteristics of a green grass (Red = 0.05, NIR = 0.40, SWIR_{1.6} = 0.25 and SWIR_{2.2} = 0.10) and a mature or senesced grass (Red = 0.15, NIR = 0.38, SWIR_{1.6} = 0.43 and SWIR_{2.2} = 0.33). The distribution of the results was similar (Fig. 5); the spectral dependence was removed by the normalisation. The results indicate that the estimation of L_ω is sufficiently independent of spectral band.

For the surface condition with reflectance of shadowed areas at 0 and lit areas at 1, we estimated ω_n and translated and scaled it to establish a calibration relation with L_c . Fig. 6 shows the relation between ω_{ns} of Marshall's roughness surfaces translated and scaled between $a = 0.0001$ and $b = 0.1$ and the L_c of those surfaces. A simple power function was fitted to these data using linear least squares regression which was statistically significant (p -value < 0.05).

4.2. Waveband selection for aerodynamic sheltering (L_ω) using MODIS black-sky albedo

For the period 2000–2015 we plotted for each location (Table 1) the ω_{ns} using f_{iso} and NBAR against each other for each of the MODIS wavebands. We found that normalising these data by NBAR produced a

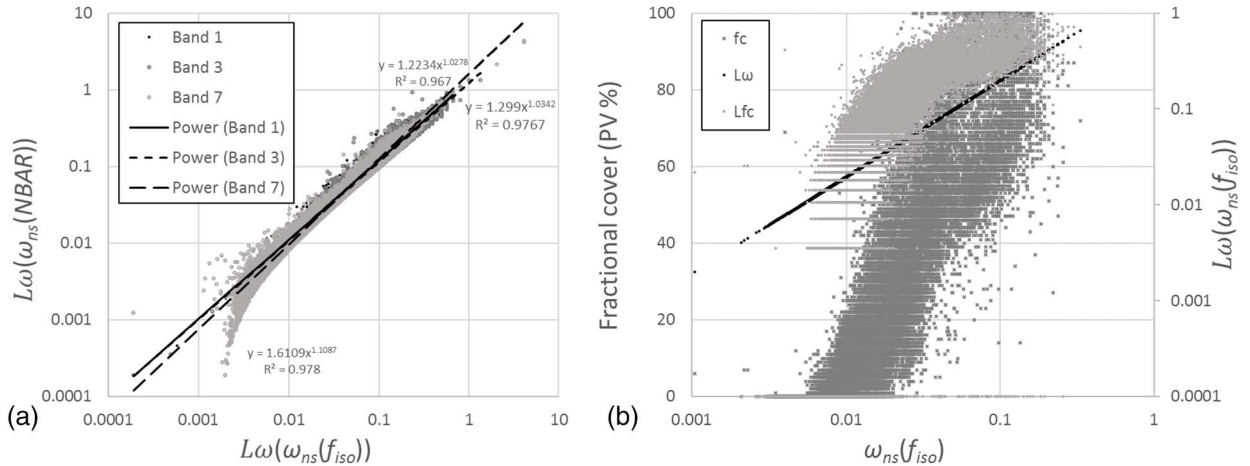


Fig. 7. Temporal data of the MODIS archive for selected pixels (cf Fig. 4) across Australia showing the MODIS black-sky albedo of band 1, 3 and 7 normalised and rescaled (ω_{ns}) using f_{iso} and NBAR (a) and MODIS band 1 normalised and rescaled using f_{iso} against fractional cover and lateral cover (L_ω and L_{fc} ; b).

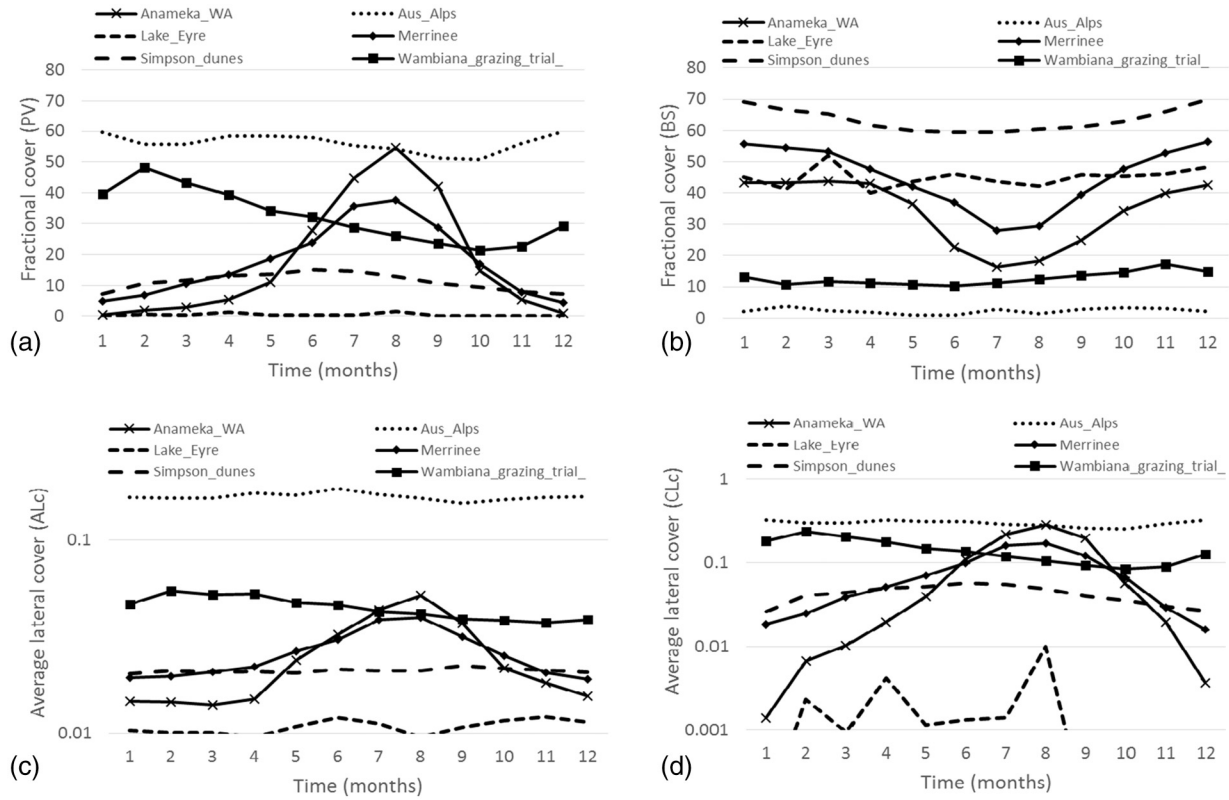


Fig. 8. Monthly cover (2000–2014; beginning with January = 1) of selected pixels across Australia from MODIS albedo (MCD43A3; 8 day, 500 m) using photosynthetic vegetation (PV, a); bare soil cover (BS, b); average lateral cover from albedo (L_{ω} , c) and from fractional cover (L_{fc} , d).

small bias and more variation than when normalised using f_{iso} . There was little difference in L_{ω} between MODIS bands (Fig. 7a). The L_{ω} for MODIS band 1 is closest to the 1:1 line (1.027) and has a similar scatter of data to MODIS band 3 ($R^2 = 0.97$). The MODIS band 7 had the greatest deviation from 1:1 (1.1) but the smallest variability ($R^2 = 0.984$). The fitted lines were statistically significant (p -value < 0.05). On this basis we decided to use MODIS band 1 with f_{iso} to calculate the ω_{ns} .

To evaluate the new method of estimating lateral cover using MODIS black sky albedo (L_{ω}) we plotted (Fig. 7b) the normalised and rescaled albedo for the time series data of the selected locations against the fractional cover (PV) and lateral cover, L_{ω} , and L_{fc} which is based on $f_c(PV)$. The straight line relation between $\omega_{ns}(f_{iso})$ and L_{ω} mimics that of the calibration (Fig. 6) and shows that the estimates of L_{ω} are consistent with the measurements from the wind tunnel study. In contrast, L_{fc} is approximately one order of magnitude too large and demonstrates a curved form (on the log-log scale) which is not evident in L_{ω} . Evidently, that shape is inherited from the form of $f_c(PV)$. In general, there is a relation between $f_c(PV)$ and L_c ; as f_c increases so too does L_c . However, for a given $f_c(PV)$ and a given L_{fc} there is considerable variation in $\omega_{ns}(f_{iso})$ which is not evident in the wind tunnel measurements. We tried using $f_c(PV + NPV)$ to represent all of the available cover but this increased the magnitude of f_c which in turn over-estimated considerably L_{fc} . In this sense, our comparison is conservative.

4.3. Temporal variation in cover

The fractional cover of photosynthetic vegetation (PV) and bare soil (BS) for selected Australian sites (Fig. 4, Table 1) are shown in Fig. 8(a & b). The largest PV occurs consistently in the Australian Alps.

The smallest occurs at Lake Eyre, an episodically dry lake bed. A consistent cover of PV with a peak in February during the growing season is also evident at Wambiana where grazing is managed to retain cover over the year. A distinct seasonal growth-related pattern in PV cover is evident at Anameka in Western Australia and Merrinee in Victoria, where wheat reaches full cover in August before being harvested (Nov/Dec) and then the stubble (represented by $NPV = 100 - PV + BS$) is grazed by sheep from Jan to Apr (wheat-sheep system). The Simpson dunes are low angle sand hills with sparse vegetation cover influenced by limited seasonal rain. Notably, the cover in these dunes is small during the summer to autumn months of November to April. The small cover during this time makes the dunes susceptible to wind erosion, particularly during strong winds towards the end of that period. (See Fig. 8.)

The time series of average lateral cover (Fig. 8c & d) for each pixel is very similar in temporal pattern to that of fractional cover of photosynthetic vegetation (PV). The temporal patterns of average lateral cover are similar in both approaches (L_{ω} and L_{fc}). However, (as shown in Fig. 7b) the L_{fc} is almost an order of magnitude larger than L_{ω} in some cases and in other cases an order of magnitude smaller. Since the L_{ω} is calibrated against measured lateral cover we can confirm that L_{fc} is incorrect.

4.4. Spatial variation of cover

To illustrate the information content of L_{ω} we evaluated it across the Interim Biogeographic Regionalisation for Australia (IBRA) and Major Land Resource Areas (MLRA) land cover classification systems for Australia and the contiguous United States, respectively (Fig. 9). The IBRA and MLRA land classification systems represent land areas with

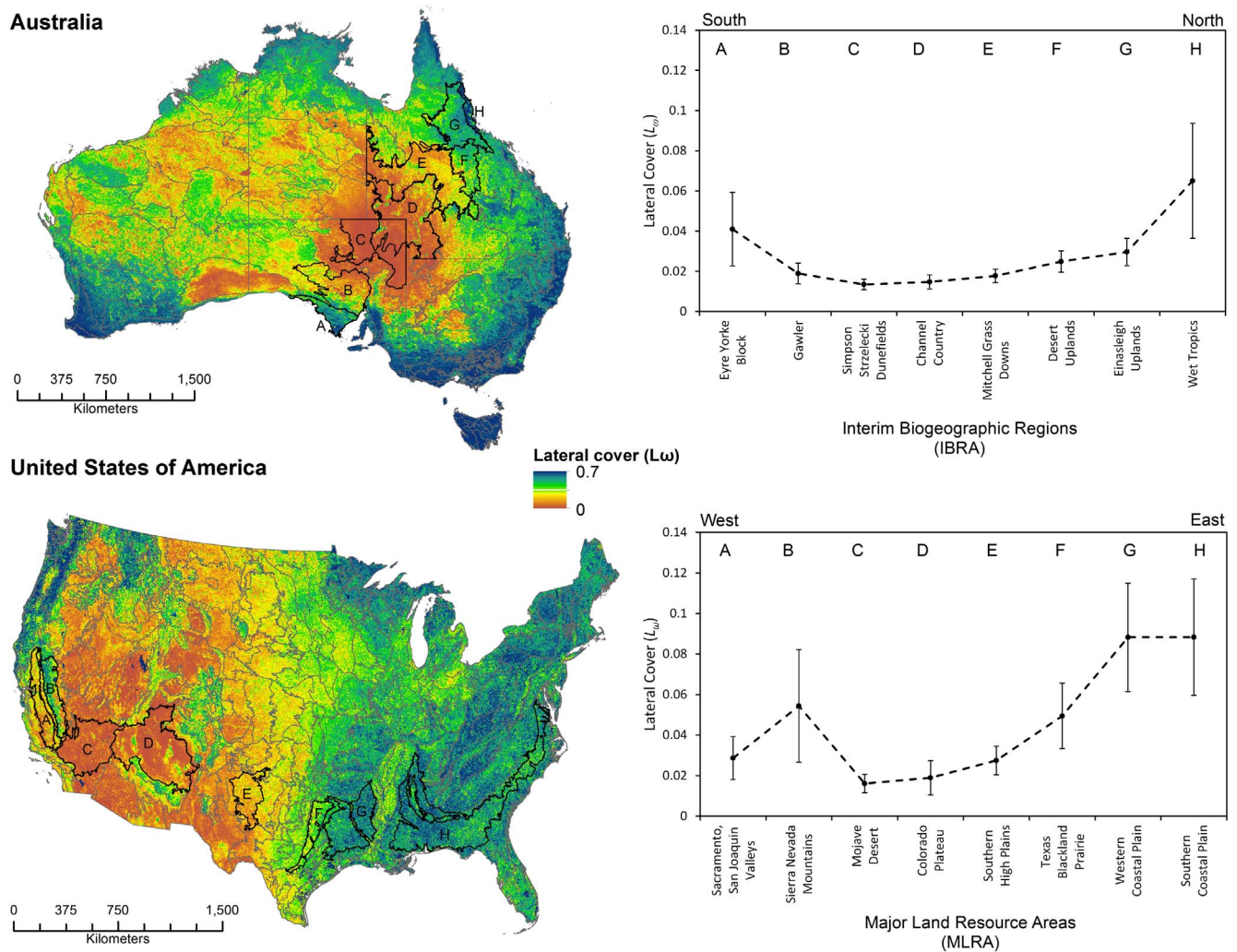


Fig. 9. MODIS-derived median lateral cover (L_w) of September 2009 for Australia and the contiguous USA with national biogeographic regions overlaid (IBRA and MLRA, respectively). The adjacent plots describe a south-north transect of L_w through the IBRA regions of Australia and a west-east transect of L_w through the MLRA regions of the USA.

similar soil, vegetation and climatic characteristics at a finer scale than the MODIS MCD12Q1 land cover classes. The systems permit interpretation of patterns of L_w at scales that are relevant to existing Australian and US monitoring and assessment programs like the Australian State of the Environment Reporting (Department of the Environment and Energy, 2016) and the US Bureau of Land Management's (BLM) Assessment, Inventory and Monitoring (AIM) Strategy (Toevs et al., 2011) and NRCs National Resources Inventory (NRI) (Goebel, 1998). We use broad transects that cut across known dust source regions to reveal the nature of AL_c patterns.

In both Australia and the US, spatial patterns of small L_w correspond with the distribution of desert rangelands and dryland cropping regions, while areas of large L_w correspond with mesic and humid regions, including mountain ranges (Fig. 9). The spatial patterns of areas with small L_w in both countries are consistent with observational records (Goudie and Middleton, 2006) and measurements (Ginoux et al., 2012) of dust source areas. These dust source areas have sparse vegetation cover relative to the more densely vegetated coastal (Australia) and eastern (US) regions that receive on average higher mean annual rainfall. In Australia, the Simpson Desert and Channel Country IBRA regions within the Lake Eyre Basin have very small L_w , and consistently

high susceptibility to wind erosion (Webb et al., 2009), relative to the savanna grasslands and shrublands of north Queensland and croplands of South Australia. In the US, an increase in L_w is evident in the transect crossing the Sierra Nevada in California, followed by a decrease in L_w through the arid southwest including the Mojave Desert and Colorado Plateau. The L_w increases from the xeric to mesic and humid MLRAs. Notably, the Southern High Plains, which befell the tragedy of the 1930's Dust Bowl (Lee and Gill (2015), has for the period of this evaluation (September 2009) small L_w and ongoing potential for wind erosion.

Detecting spatial and temporal change in L_w provides the capability to more precisely monitor wind erosion potential in areas such as the Southern High Plains MLRA (Fig. 10). Patterns of wind erosion in space and time are driven by localised variations in surface aerodynamic roughness (i.e., L_w) that result from patterns of soils and vegetation responses to rainfall and grazing in rangelands, and the timing of tillage, sowing and harvesting operations in croplands. Detecting the effects of these changes, and changes in land use (e.g. rangeland to cropland conversion) more broadly, for wind erosion monitoring is difficult using fractional vegetation cover alone (Section 1), but can now be achieved using L_w at management-relevant scales that enable

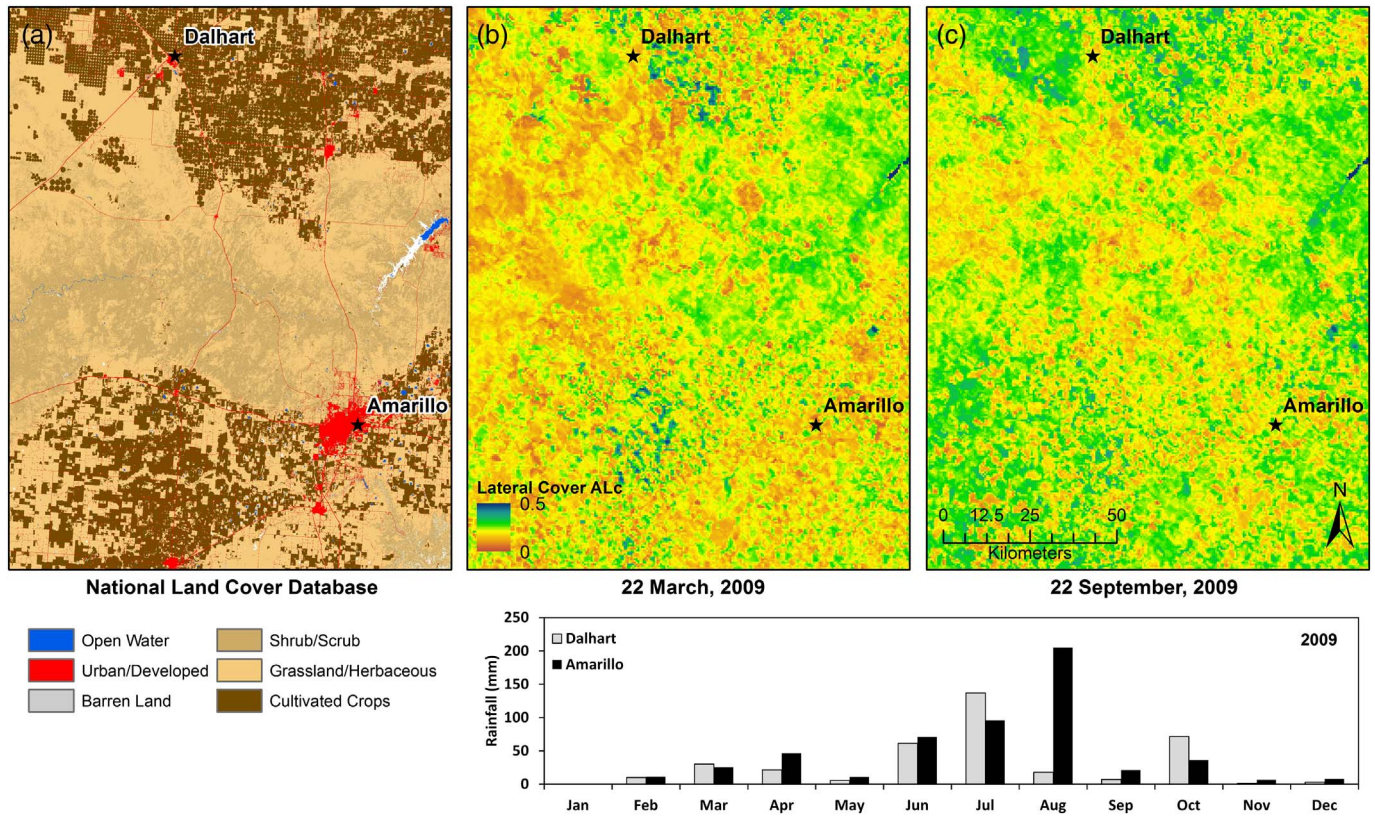


Fig. 10. For a part of the Southern High Plains Major Land Resource Area (MLRA), the MODIS National Land Cover Database (Homer et al., 2015; <http://www.mrlc.gov/nlcd2011.php>) reveals the extent of croplands and mixed grasslands and shrublands between Dalhart and Amarillo, Texas, USA (a). MODIS-derived lateral cover (L_{ω}) for the same MLRA shows seasonal changes in surface aerodynamic roughness between (b) the approximate crop planting period and (c) prior to harvest. Inset graph shows monthly rainfall for 2009.

monitoring in both time (Fig. 8) and space (Fig. 10). Heterogeneity in L_{ω} is large in both the rangelands and croplands, while the cropland management practices create distinct patterns of surface aerodynamic roughness – in this case reflecting the predominant use of centre-pivot irrigation systems around Dalhart and Amarillo.

5. Discussion

5.1. Removing the spectral influences of lateral cover

One of the main achievements of this work is to demonstrate that the spectral confounding factors (soil composition and moisture) can be removed to isolate the structural contribution. Weidong et al. (2002) normalised soil reflectance spectra by that of a dry condition to minimise the effects due to soil type and other ‘undesirable’ multiplicative factors such as roughness and measurement configuration. Our initial investigation of this approach worked well with our ray-casting experiments but when applied to MODIS data, it created considerable noise due to the selection of the maximum black-sky albedo of the pixels. In situations where there is no change in the roughness over time this approach would work. However, we found that in many situations the roughness would change either naturally during the seasons or in response to land use and management practices. Consequently, this approach did not normalise to the driest condition but to the brightest condition, which itself may be due to either changes in roughness, soil composition or moisture. For these reasons, the approach of Weidong et al. (2002) was not used in our investigation.

We demonstrated using our ray-casting simulations that the normalisation of the at-nadir hemispherical ‘black-sky’ albedo $\omega_{dir}(\theta, \lambda)$ does work. We tested this with MODIS data and the ratio with either the spectral BRDF parameter f_{iso} or using NBAR. Both approaches performed well. The former approach using f_{iso} performed slightly better.

This outcome was expected since f_{iso} contains the majority of the spectral signature from the BRDF modelling. We know a priori that $\omega_{dir}(\theta, \lambda)$ is dependent on waveband (e.g., Pinty et al., 1989) and so we tested the normalisation with three MODIS wavebands. We found that the normalisation removed the influence of waveband such that any waveband could be used. Statistically, we found a small benefit from using MODIS band 1 (620–670 nm). These findings have two implications. Firstly, other workers can use the readily available MODIS BRDF parameters to estimate L_{ω} . It also means that ground measurements of albedo for any given waveband (e.g., on an instrumented tower) can be divided by the albedo at, or around, solar-noon to normalise and estimate L_{ω} .

5.2. Advantages of lateral cover (L_{ω}) over existing metrics

Remotely-sensed monitoring products provide variation in green cover, normalised difference vegetation index (NDVI) and other similar green vegetation indices which may be unrelated to land management practices particularly in dry, seasonal environments like those of Australia. For example, Scarth et al. (2010) showed that fractional cover (f_c) and non-photosynthetic cover offers considerable benefits in this respect. Although valuable for studies of vegetation dynamics, fractional cover and other available vegetation indices do not adequately assess the protection of the land surface roughness against wind erosion. Current approaches to estimating L_c using satellite remote sensing data are hindered by the need to translate from leaf area index (LAI) or NDVI data. They require additional information about the vegetation characteristics, such as height and shape, which are typically derived from land cover classifications. The LAI and NDVI are more sensitive to the physiological rather than physical state of vegetation, which also complicates the estimation of L_c from these data. Furthermore, the L_c was derived from an empirical relation with a single

vegetation cover (wheat-stubble; Shao et al., 1996). However, this empirical relation has never been replicated or tested under different cover types and configurations. Our new approach based on albedo accounts for the structure and configuration of the land surface roughness and avoids arbitrary land surface classifications in the estimation of L_c . Our new method of estimating lateral cover provides a physically-based approximation of the area of soil downwind of an obstacle protected from the shearing forces of the wind. We established a functional relation for L_ω using measured L_c and rescaled ω_{ns} . We also calculated the lateral cover using fractional cover (L_{fc}) following existing approaches to modelling wind erosion. Our new approach therefore provides a robust approximation which updates the current approaches to the estimation of L_c .

The estimates of L_ω and L_{fc} are difficult to validate because ground measurements of L_c are not available but also because many samples or smart sampling designs are required to reduce uncertainty in the measurements. This dearth of data is partly because of the lack of awareness of the L_c metric outside the aeolian research community, but mainly because of the time-consuming nature of the measurements necessary to estimate L_c , particularly over large areas. We found that L_ω was similar to L_{fc} but the latter was an order of magnitude too small or too large depending on plant phenological stage. Since L_ω was calibrated with geometric measurements from wind tunnel experiments, the differences with L_{fc} are interpreted here as the result of the crude approximation of the L_{fc} parameterisation. Among other things, the single value for the roughness element shape coefficient used by L_{fc} is a poor approximation of the three-dimensional nature of the roughness and sheltering areas. We found L_ω to be similar to f_c in temporal patterns. That similarity shows that f_c provides an approximation of the planform area of exposed soil that may be susceptible to wind erosion. However, that approximation is far-removed from the sheltering effects of surface roughness on sediment transport by wind (cf Shao, 2000). Since lateral cover is closely related to wind erosion, we can be more confident with L_ω than with fractional cover that we are assessing the susceptibility to wind erosion. In other words, when lateral cover is small, e.g., prior to and during seedling emergence or during stubble grazing, we can be confident that a field is vulnerable to wind erosion. It follows then that the dynamics of ground cover monitoring for wind erosion assessment using our MODIS-based approach should at least be complemented by the estimation of lateral cover.

5.3. Monitoring lateral cover (L_ω) for wind erosion assessment

The recent interest, particularly in Australia and the USA, of monitoring national ground cover for wind erosion assessment has focused on satellite remote sensing (Australia) or field measurement (USA) of fractional cover and culminated in national evaluations of methods (e.g. Mackinnon et al., 2011). The benefits of satellite remote sensing for national monitoring are well-established in providing relatively cheap, consistent and repeatable estimates over large areas. However, in common with many applications of remote sensing, the retrievals are surrogates of the information that is actually required. Fractional cover (f_c) provides valuable information about the planform cover of the BS, PV and NPV proportions of ground covered in a pixel. However, f_c provides no information about the vertical structure of these cover types. The implications for wind erosion are illustrated well in the case of wheat crop residues, where upright stems rooted in the soil offer greater soil protection, with smaller fractional cover, compared with loose stems lying flat against the ground. Consequently, f_c provides only a crude approximation of the sheltering and protection from wind erosion provided by ground cover. Lateral cover (L_c) is more closely related to wind erosion than fractional cover. The results from our study indicate that L_c contains information that is applicable to monitoring wind erosion and which is not available from f_c . Consequently, we suggest that our albedo-based estimate L_ω should be used particularly for regional to national assessments of wind erosion to provide a direct

relation with the lateral forces of wind.

An operational method for estimating L_c exists for the national Australian dust emission monitoring program that makes use of the Computational Environmental Management System (CEMSYS) model. The work presented here demonstrates that CEMSYS and other wind erosion and dust emission models, including those implemented in regional and global models based on current lateral cover approximations, are likely to be highly uncertain. Models which adopt the albedo-based approach can directly and continuously estimate the dynamics of L_c over space and time. Consequently, this new approach should reduce considerably the inferences required for the wind erosion and dust emission models to estimate L_c and hence reduce uncertainty in wind erosion assessment and dust emission modelling.

In the USA, there is great awareness of the recurrent, pervasive and degrading nature of wind erosion and its consequences for soil health and ultimately food security. A National Wind Erosion Research Network has recently been established (Webb et al., 2016) and complements the already considerable resources, particularly field measurements, that are used to monitor the condition of agricultural and rangeland environments (e.g., the AIM and NRI programs). Our new approach provides a dynamic (multi-temporal), moderate resolution and global metric for wind erosion assessment and modelling. It offers the potential for cost-effective routine monitoring of vegetation dynamics in space and time. Perhaps the greatest potential use is for wind erosion assessment and monitoring soil degradation in developing countries. The combination of available MODIS satellite data and Google Earth Engine processing, provides an unprecedented and readily accessible tool for countries without the resources for field monitoring.

5.4. Limitations of the new approach to estimating lateral cover (L_ω)

The traditional approach to estimating L_c is used for regional and global wind erosion and dust emission modelling (Shao et al., 1996). The estimates of L_c in that approach are typically based on a vegetation index or may use fractional cover, as we have shown here (L_{fc}). That traditional approach is calibrated to measurements made on one field in Australia. There have been very few studies which have validated estimates of L_c and only within a single field (Marticorena et al., 2006; Pierre et al., 2014). Our new approach L_ω is similarly limited by the dearth of ground measurements. By comparison with traditional approaches, L_ω can be evaluated more readily because of its dependency on albedo and the straightforward way that it can be scaled. Consequently, measurements of albedo close to the ground e.g., mounted on meteorological towers, can be compared directly with field measurements of L_c within the field of view (e.g., Webb et al., 2016). The proximity to the ground of the albedo measurement enables small (relatively homogeneous) land surface (vegetation) types to be measured. For the same limited ground-based sampling resources, more samples would be available between land surface (vegetation) types. Hence, the use of albedo enables estimation of L_ω across scales over small areas and thereby improves the likelihood that sampling designs will represent both the within-class and between-class variance and adequately represent the total variance.

6. Conclusions

Our work provides the following findings and recommendations particularly for regional and continental scale wind erosion assessments important for resource management agencies and policy-makers:

- 1) Ground cover monitoring for wind erosion assessment requires information about the lateral cover of vegetation. Fractional cover is useful to interpret the type of cover. Lateral cover is sensitive to change in vegetation height associated with plant phenological stage and seasonal land cover and land management change.
- 2) We developed a physical or process-based relation between lateral

- cover and shadow as an approximation of the area sheltered from the wind downwind of the land surface roughness (vegetation). That relation acted as a calibration of MODIS albedo once those data were converted to shadow and normalised to remove the spectral influences. This methodology formed a new approach to routine estimates of lateral cover using albedo data from field measurements or satellite remote sensing.
- 3) Current approximations of lateral cover (parameterisations based on NDVI or fractional cover) were found to be poorly developed by comparison with the new calibrated approach based on measurements of lateral cover.
 - 4) With the support of the Google Earth Engine, we have processed the MODIS albedo data archive to produce global estimates of lateral cover (with the same spatial and temporal resolution). The code for this methodology is straightforward and available and can enable these data to be readily applied in developing countries or where resources are limited for wind erosion monitoring and modelling.
 - 5) We expect that remote sensing of L_c will enable resource management agencies and policy-makers to make more informed decisions about how to maintain roughness of ground cover and thereby reduce wind erosion.
 - 6) The traditional approach to estimating L_c was unvalidated because of the dearth in ground-based measurements specifically required for its validation. That limitation remains the main weakness of our new approach. While we have shown how our new approach has improved on the traditional approach, it requires validation. Our improvements mean that the new estimates of lateral cover L_w will reduce uncertainty in sediment transport and dust emission models.
 - 7) Future work should consider including the dependency of the sheltered soil surface area on wind speed since this influences the downstream area of bare ground that is exposed to potentially erosive winds.

Acknowledgements

Funding from the Australian Wool Innovation Ltd for a project on 'Increasing wool sheep in cropping zones' provided the time for some of the authors to work on this manuscript. We also acknowledge support from the USDA Natural Resources Conservation Service, Conservation Effects Assessment Project to develop new wind erosion decision-support tools. We are grateful to NASA LP DAAC at the USGS EROS Center for the provision of MODIS data and to Google for access to the Earth Engine (GEE) for processing and data manipulation. We thank Dr. Tim McVicar and Prof. Albert Van Dijk for their constructive comments on the manuscript. Any errors or omissions are the responsibility of the authors. The GEE javascript code for processing the MODIS data to retrieve lateral cover is available by contacting the first author.

References

ABARES, 2012. Ground Cover Reference Sites Database. Australian Bureau of Agricultural and Resource Economics and Sciences, Canberra, Australia. <https://rs.nci.org.au/FcSiteData/>.

Arya, S.P.S., 1975. A drag partition theory for determining the large-scale roughness parameter and wind stress on the Arctic Pack Ice. *J. Geophys. Res.* 80, 3447–3454.

Bergametti, G., Gillette, D.A., 2010. Aeolian sediment fluxes measured over various plant/soil complexes in the Chihuahuan desert. *J. Geophys. Res.* 115 (F03044), 2010. <http://dx.doi.org/10.1029/2009JF001543>.

den Biggelaar, C., Lal, R., Wiebe, K., Eswaran, H., Breneman, V., 2003a. The global impact of soil erosion on productivity. I. Absolute and relative erosion-induced yield losses. *Adv. Agron.* 81, 1–48.

den Biggelaar, C., Lal, R., Wiebe, K., Eswaran, H., Breneman, V., 2003b. The global impact of soil erosion on productivity. II. Effects on crop yield and production over time. *Adv. Agron.* 81, 49–95.

Brown, S., Nickling, W.G., Gillies, J.A., 2008. A wind tunnel examination of shear stress partitioning for an assortment of surface roughness distributions. *J. Geophys. Res.* 113, F02S06. <http://dx.doi.org/10.1029/2007JF000790>.

Calvo, E., Pelejero, C., Logan, G.A., De Deckker, P., 2004. Dust-induced changes in phytoplankton composition in the Tasman Sea during the last four glacial cycles. *Palaeoceanography* 19, PA2020. <http://dx.doi.org/10.1029/2003PA000992>.

Chappell, A., Heritage, G.L., 2007. Using illumination and shadow to model aerodynamic resistance and flow separation: an isotropic study. *Atmos. Environ.* 41 (28), 5817–5830. <https://doi.org/10.1016/j.atmosenv.2007.03.037>.

Chappell, A., Zobeck, T.M., Brunner, G., 2006. Using bi-directional soil spectral reflectance to model soil surface changes induced by rainfall and wind-tunnel abrasion. *Remote Sens. Environ.* 102 (3–4), 328–343. <https://doi.org/10.1016/j.rse.2006.02.020>.

Chappell, A., Strong, C., McTainsh, G., Leys, J., 2007. Detecting induced in situ erodibility of a dust-producing playa in Australia using a bi-directional soil spectral reflectance model. *Remote Sens. Environ.* 106, 508–524. <https://doi.org/10.1016/j.rse.2006.09.009>.

Chappell, A., Dong, Z., Van Pelt, S., Zobeck, T., 2010. Estimating aerodynamic resistance of rough surfaces using angular reflectance. *Remote Sens. Environ.* 114 (7), 1462–1470. <https://doi.org/10.1016/j.rse.2010.01.025>.

Chappell, A., Webb, N.P., Butler, H.J., Strong, C.L., McTainsh, G.H., Leys, J.F., Viscarra Rossel, R.A., 2013. The role of carbon dust emission as a global source of atmospheric CO₂. *Glob. Chang. Biol.* 19, 3238–3244. <https://doi.org/10.1111/gcb.12305>.

Cho, J., Miyazaki, S., Yeh, P.J.-F., Kim, W., Kanae, S., Oki, T., 2012. Testing the hypothesis on the relationship between aerodynamic roughness length and albedo using vegetation structure parameters. *Int. J. Biometeorol.* 56, 411–418. <http://dx.doi.org/10.1007/s00484-011-0445-2>.

Cierniewski, J., 1987. A model for soil surface roughness influence on the spectral response of bare soils in the visible and near-infrared range. *Remote Sens. Environ.* 23, 97–115.

Coulson, K.L., Reynolds, D.W., 1971. The spectral reflectance of natural surfaces. *J. Appl. Meteorol.* 10, 1285–1295.

Darmenova, K., Sokolik, I.N., Shao, Y., Marticorena, B., Bergametti, G., 2010. Development of a physically based dust emission module within the Weather Research and Forecasting (WRF) model: Assessment of dust emission parameterizations and input parameters for source regions in Central and East Asia. *J. Geophys. Res.* 114, D14201. <http://dx.doi.org/10.1029/2008JD011236>.

Department of the Environment and Energy, 2016. National State of the Environment (SoE) reporting. Online resource: <https://www.environment.gov.au/science/soe> (Accessed: August, 2016).

Dickinson, R.E., 1983. Land surface processes and climate surface albedos and energy-balance. *Adv. Geophys.* 25, 305–353. [http://dx.doi.org/10.1016/S0065-2687\(08\)60176-4](http://dx.doi.org/10.1016/S0065-2687(08)60176-4).

Dong, Z., Liu, X., Wang, X., 2002. Aerodynamic roughness of gravel surfaces. *Geomorphology* 43 (1–2), 17–31.

Felton, W., Freebairn, D.M., Fettel, N.A., Thomas, J., 1987. Crop residue management. In: Cornish, P.S., Pratley, J.E. (Eds.), *Tillage*. Melbourne, Inkata Press, pp. 171–193.

Friedl, M.A., Sulla-Menashe, D., Tan, B., Schneider, A., Ramankutty, N., Sibley, A., Huang, X., 2010. MODIS Collection 5 global land cover: Algorithm refinements and characterization of new datasets, 2001–2012. In: *Collection 5.1 IGBP Land Cover*, Boston University, Boston, MA, USA.

Gillette, et al., 2006. Wind characteristics of mesquite streets in the Northern Chihuahuan Desert, New Mexico, USA. *Environ. Fluid Mech.* 6, 241–275.

Ginoux, P., Prospero, J.M., Gill, T.E., Hsu, N.C., Zhao, M., 2012. Global-scale attribution of anthropogenic and natural dust sources and their emission rates based on MODIS Deep Blue aerosol products. *Rev. Geophys.* 50, RG3005.

Goebel, J.J., 1998. The National Resources Inventory and its role in U.S. Agriculture, agricultural statistics 2000. In: *Proceedings of the Conference on Agricultural Statistics Organized by the National Agricultural Statistics Service of the U.S.* Department of Agriculture, Under the Auspices of the International Statistical Institute, pp. 181.

Goudie, A., Middleton, N.J., 2006. *Desert Dust in the Global System*. Springer-Verlag Berlin Heidelberg.

Guerschman, J.P., Hill, M.J., Renzullo, L.J., Barrett, D.J., Marks, A.S., Botha, E.J., 2009. Estimating fractional cover of photosynthetic vegetation, non-photosynthetic vegetation and bare soil in the Australian tropical savanna region upscaling the EO-1 Hyperion and MODIS sensors. *Remote Sens. Environ.* 113 (5), 928–945. <http://dx.doi.org/10.1016/j.rse.2009.01.006>.

Guerschman, Juan, Scarth, Peter, McVicar, Tim, Renzullo, Luigi, Malthus, Tim, Stewart, Jane, et al., 2015. Assessing the effects of site heterogeneity and soil properties when unmixing photosynthetic vegetation, non-photosynthetic vegetation and bare soil fractions from Landsat and MODIS data. *Remote Sens. Environ.* 161 (1), 12–26.

Hapke, B., 1993. *Theory of reflectance and emittance spectroscopy*. Cambridge Univ. Press, Cambridge, UK.

Herrick, J.E., Van Zee, J.W., McCord, S.E., Courtright, E.M., Karl, J.W., Burkett, L.M., 2017. *Monitoring manual for grassland, shrubland, and savanna ecosystems*. In: *Core Methods*, second ed. vol. 1 USDA-ARS Jornada Experimental Range, Las Cruces, New Mexico.

Homer, C.G., Dewitz, J.A., Yang, L., Jin, S., Danielson, P., Xian, G., Coulston, J., Herold, N.D., Wickham, J.D., Megown, K., 2015. Completion of the 2011 National Land Cover Database for the conterminous United States-Representing a decade of land cover change information. *Photogramm. Eng. Remote Sens.* 81 (5), 345–354.

Huang, J., Yu, H., Guan, X., Wang, G., Guo, R., 2016. Accelerated dryland expansion under climate change. *Nat. Clim. Chang.* 6, 166–171. <http://dx.doi.org/10.1038/nclimate2837>.

Jacquemoud, S., Bater, F., Hanocq, J.F., 1992. Modeling spectral and bidirectional soil reflectance. *Remote Sens. Environ.* 41, 123–132.

Jickells, T.D., et al., 2005. Global iron connections between dust, ocean biogeochemistry and climate. *Science* 308, 67–71.

Koch, A., Chappell, A., Eyres, M., Scott, E., 2015. Monitor soil degradation or triage for soil security? An Australian challenge. *Sustainability* 2015 (7), 4870–4892. <https://doi.org/10.3390/su7054870>.

- Lal, R., 1998. Soil erosion: impact on agronomic productivity and environmental quality. *Crit. Rev. Plant Sci.* 17, 319–464.
- Lal, R., 2001. Soil degradation by erosion. *Land Degrad. Dev.* 12, 519–539.
- Lee, J.A., Gill, T.E., 2015. Multiple causes of wind erosion in the Dust Bowl. *Aeolian Res.* 19 (A), 15–36. <http://dx.doi.org/10.1016/j.aeolia.2015.09.002>.
- Leys, J.F., 1991. Towards a better model of the effect of prostrate vegetation cover on wind erosion. *Vegetatio* 91, 49–58.
- Leys, J.F., Smith, J., MacRae, C., Rickards, J., Yang, X., Randall, L., Hairsine, P., Dixon, J., McTainsh, G., 2009. Improving the Capacity to Monitor Wind and Water Erosion: A Review. Department of Agriculture, Fisheries and Forests, Australian Government, Canberra (160 pp.). available at: www.nrm.gov.au/publications/books/pubs/wind-water-erosion.pdf.
- Li, J., Okin, G.S., Alvarez, L., Epstein, H., 2007. Quantitative effects of vegetation cover on wind erosion and soil nutrient loss in a desert grassland of southern New Mexico, USA. *Biogeochemistry* 85, 317–332.
- Li, et al., 2008. Effects of wind erosion on spatial heterogeneity of soil nutrients in two desert grassland communities. *Biogeochemistry* 88, 73–88.
- Lucht, W., Schaaf, C.B., Strahler, A.H., 2000. An algorithm for the retrieval of albedo from space using semi-empirical BRDF models. *IEEE Trans. Geosci. Remote. Sens.* 38 (2), 977–998.
- Mackinnon, W., Karl, J.W., Taylor, J., Karl, M., Spurrier, C., Herrick, J.E., 2011. BLM Core Terrestrial Indicators and Methods: Technical Note 440. US Department of the Interior, Bureau of Land Management, National Operations Center, Denver, CO.
- Marshall, J.K., 1971. Drag measurements in roughness arrays of varying density and distribution. *Agric. Meteorol.* 8, 269–292.
- Marticorena, B., Bergametti, G., 1995. Modeling the atmospheric dust cycle: 1. Design of a soil-derived dust emission scheme. *J. Geophys. Res.* 100 (D8), 16415–16430.
- Marticorena, B., Kerdous, M., Bergametti, G., Callot, Y., Chazette, P., Khatteli, H., Le He'garat-Masclé, S., Maillé, M., Rajot, J.-L., Vidal-Madjar, D., Zribi, M., 2006. Surface and aerodynamic roughness in arid and semiarid areas and their relation to radar backscatter coefficient. *J. Geophys. Res.* 111, F03017. <http://dx.doi.org/10.1029/2006JF000462>.
- McTainsh, G., Lynch, A., Burgess, R., 1990. Wind erosion in eastern Australia. *Aust. J. Soil Res.* 28, 323–339.
- Monteith, J.L., Unsworth, M.H., 2008. *Principles of Environmental Physics*, 3rd ed. Academic Press.
- Muir, J., Schmidt, M., Tindall, D., Trevithick, R., Scarth, P., Stewart, J., 2011. Guidelines for field measurement of fractional ground cover: a technical handbook supporting the Australian collaborative land use and management program. In: Tech. Rep. Queensland Department of Environment and Resource Management for the Australian Bureau of Agricultural and Resource Economics and Sciences, Canberra.
- Pierre, C., Bergametti, G., Marticorena, B., Kergoat, L., Mougou, E., Hiernaux, P., 2014. Comparing drag partition schemes over a herbaceous Sahelian rangeland. *J. Geophys. Res. Earth Surf.* 119, 2291–2313. <http://dx.doi.org/10.1002/2014JF003177>.
- Pinty, B., Verstraete, M.M., Dickinson, R.E., 1989. A physical model for predicting bidirectional reflectances over bare soil. *Remote Sens. Environ.* 27, 273–288.
- Raupach, M.R., 1992. Drag and drag partition on rough surfaces. *Bound.-Layer Meteorol.* 60, 374–396.
- Raupach, M.R., Gillette, D.A., Leys, J.F., 1993. The effect of roughness elements on wind erosion thresholds. *J. Geophys. Res.* 98, 3023–3029.
- Ravi, et al., 2010. Land degradation in drylands: interactions among hydrologic-aeolian erosion and vegetation dynamics. *Geomorphology* 116, 236–245.
- Roujean, J.L., Leroy, M., Deschamps, P.Y., 1992. A bidirectional reflectance model of the Earth's surface for the correction of remote sensing data. *J. Geophys. Res.* 97, 20455–20468.
- Scarth, P., Roder, A., Schmidt, M., 2010. Tracking grazing pressure and climate interaction—the role of Landsat fractional cover in time series analysis. In: Proceedings of the 15th Australasian Remote Sensing and Photogrammetry Conference, available at: www.scribd.com/doc/37455672/15arspc-Submission-140.
- Schaaf, C.B., Gao, F., Strahler, A.H., Lucht, W., Li, X.W., Tsang, T., et al., 2002. First operational BRDF, albedo nadir reflectance products from MODIS. *Remote Sens. Environ.* 83, 135–148.
- Shao, Y., 2000. *Physics and modelling of wind erosion*. Kluwer Academic, London.
- Shao, Y., Raupach, M.R., Leys, J.F., 1996. A model for predicting aeolian sand drift and dust entrainment on scales from paddock to region. *Aust. J. Soil Res.* 34, 309–342.
- Shao, Y., Leys, J., McTainsh, G., Tews, K., 2007. Numerical simulation of the October 2002 dust event in Australia. *J. Geophys. Res.* 112, 1–12.
- Shao, Y., Wyrwoll, K.-H., Chappell, A., Huang, J., Lin, Z., McTainsh, G., Mikami, M., Tanaka, T., Wang, X., Yoon, S., 2011. Dust cycle: an emerging core theme in Earth system science. *Aeolian Res.* 2 (4), 181–204. <https://doi.org/10.1016/j.aeolia.2011.02.001>.
- State of the Environment 2011 Committee, 2011. Australia state of the environment 2011. In: Independent Report to the Australian Government Minister for Sustainability, Environment, Water, Population and Communities. DSEWPac, Canberra, pp. 2011.
- Sterk, G., Herrmann, L., Bationo, A., 1996. Wind-blown nutrient transport and soil productivity changes in southwest Niger. *Land Degrad. Dev.* 7 (4), 325–335.
- Stewart, J.B., Rickards, J.E., Bordas, V.M., Randall, L.A., Thackway, R.M., 2011. Ground cover monitoring for Australia – establishing a coordinated approach to ground cover mapping. In: Workshop proceedings Canberra 23–24 November 2009. March ABARES, Canberra available at: dl.brs.gov.au/data/warehouse/pe_abaes99001799/Groundcover_mapping-workshop_proc_11.pdf.
- Toews, G.R., Karl, J.W., Taylor, J.T., Spurrier, C.S., Karl, M., Bobo, M.R., Herrick, J.E., 2011. Consistent indicators and methods and a scalable sample design to meet assessment, inventory, and monitoring information needs across scales. *Rangelands* 33, 14–20.
- Tsvetinskaya, E.A., Schaaf, C.B., Gao, F., Strahler, A.H., Dickinson, R.E., Zeng, X., Lucht, W., 2002. Relating MODIS-derived surface albedo to soils and rock types over Northern Africa and the Arabian peninsula. *Geophys. Res. Lett.* 29 (9), 1353. <http://dx.doi.org/10.1029/2001GL014096>.
- U.S. Department of Agriculture, 2015. Summary Report: 2012 National Resources Inventory. Natural Resources Conservation Service, Washington, DC, and Center for Survey Statistics and Methodology, Iowa State University, Ames, Iowa. <http://www.nrcs.usda.gov/technical/nri/12summary>.
- U.S. Department of Agriculture, Natural Resources Conservation Service (USDA NRCS), 2006. Land Resource Regions and Major Land Resource Areas of the United States, the Caribbean, and the Pacific Basin. U.S. Department of Agriculture Handbook. 296.
- Walter, B., Gromke, C., Lehning, M., 2012. Shear-stress partitioning in live plant canopies and modifications to Raupach's model. *Bound.-Layer Meteorol.* 144, 217–241.
- Wanner, W., Li, X., Strahler, A.H., 1995. On the derivation of kernels for kernel-driven models of bidirectional reflectance. *J. Geophys. Res.* 100 (D10), 21077–21089.
- Webb, N.P., Strong, C.L., 2011. Soil erodibility dynamics and its representation for wind erosion and dust emission models. *Aeolian Res.* 3, 165–179.
- Webb, N.P., McGowan, H.A., Phinn, S.R., McTainsh, G.H., Leys, J.F., 2009. Simulation of the spatiotemporal aspects of land erodibility in the northeast Lake Eyre Basin, Australia, 1980–2006. *J. Geophys. Res. Earth Surf.* 114, F01013. <http://dx.doi.org/10.1029/2008JF001097>.
- Webb, N.P., Chappell, A., Strong, C., Marx, S., McTainsh, G., 2012. The significance of carbon-enriched dust for global carbon accounting. *Glob. Chang. Biol.* <http://dx.doi.org/10.1111/j.1365-2486.2012.02780.x>.
- Webb, N.P., Okin, G.S., Brown, S., 2014. The effect of roughness elements on wind erosion: the importance of surface shear stress distribution. *J. Geophys. Res.-Atmos.* 119, 6066–6084.
- Webb, N.P., Herrick, J., Van Zee, J., Courtright, E., Hugenholtz, C., Zobeck, T.M., Okin, G.S., Barchyn, T.E., Billings, B.J., Boyd, R., Clingan, S., Cooper, B., Duniway, M.C., Derner, J.D., Fox, F.A., Havstad, K.M., Heilman, P., LaPlante, V., Ludwig, N.A., Metz, L.J., Nearing, M.A., M. Norfleet, L., Pierson, F.B., Sanderson, M.A., Sharratt, B.S., Steiner, J.L., Tatarko, J., Tedela, N.H., Toledo, D., Unnasch, R.S., R. Van Pelt, S., Wagner, L., 2016. The National Wind Erosion Research Network: Building a standardized long-term data resource for aeolian research, modeling and land management. *Aeolian Res.* 22, 23–36.
- Weidong, L., Baret, F., Xingfa, G., Qingxi, T., Lanfen, Z., Bing, Z., 2002. Relating soil surface moisture to reflectance. *Remote Sens. Environ.* 81, 238–246.